J. Micromech. Microeng. **17** (2007) S197–S203 doi:10.1088/0960-1317/17/7/S18

A dual-side fabrication method for silicon plate springs with high out-of-plane stiffness

S L Paalvast[1], H W van Zeijl[2], J Su[2,3], P M Sarro[2] and J van Eijk[1]

[1] Delft University of Technology/3mE, Mekelweg 2, 2628CD Delft, The Netherlands
[2] Delft University of Technology/DIMES, Feldmannweg 17, 2628CT Delft, The Netherlands

E-mail: S.L.Paalvast@tudelft.nl

Received 8 January 2007, in final form 7 June 2007
Published 2 July 2007
Online at stacks.iop.org/JMM/17/S197

Abstract
Guiding mechanisms guide the motion of a rigid body along a precisely defined path. For small motions flexible elements are well suited to act as joints of a guiding mechanism. Such joints must have high compliance in one, or more, direction(s), while simultaneously having high stiffness in the other directions. Plate springs meet this requirement, but the support stiffness varies per direction. For micro systems such as gyroscopes, microactuators for hard disk drives, and sample stages for high resolution microscopy, it is desirable to have the highest stiffness perpendicular to the direction, or plane, of motion. This increases the accuracy of the motion and makes the device more robust. In this work we present a fabrication method for such high out-of-plane stiffness plate springs. These high aspect ratio springs are designed and fabricated in silicon using a combination of two technologies: dual-side wafer stepper alignment and deep reactive ion etching. The plate springs are characterized by resonance frequency measurements. A model of the plate spring is fitted to the measurement data to discriminate tolerances of the two technologies used in the fabrication process.

1. Introduction

In precision engineering, plate springs are commonly used construction elements for accurate guiding mechanisms. Upon actuation, such mechanisms guide the motion of a rigid body along a precisely defined path. In situations where only small relative motions are required, flexible elements (e.g., springs) are good alternatives as the joints of a guiding mechanism. These flexure mechanisms are ideal for monolithic fabrication and do not suffer from friction and backlash. Since the required constraints and freedoms are in different directions, the flexible joint must have a high compliance in one, or more, direction(s), while simultaneously having high stiffness in the other directions. Plate springs (figure 1) are useful flexible joints, because they have high stiffness for translations in the x- and z-directions and for rotations around the y-axis, while at the same time having high compliance for translation in the y-direction and rotations around the x- and z-axis.

With the silicon-based miniaturization of sensors and actuators, the use of flexible guiding mechanisms has been extended to the silicon micro domain. Many examples of micro systems based on plate springs, or comparable flexible joints, can be found in literature, for instance a gyroscope [1], an optical switch [2], a tuning element for an external cavity laser [3], an electro-thermal micromotor [4], a microactuator for hard disk drives [5], and a positioning stage for high resolution microscopy [6]. For these examples it is important to constrain undesired motion directions with high stiffness, for instance to avoid cross-talk in a gyroscope or to prevent alignment errors in an optical switch. Also, high suspension stiffness makes the device more robust for external forces (reduced strain), such as the air bearing force in a hard disk drive, or the forces that work on a microscope positioning stage when (dis-)mounting a sample.

[3] Current address: IMEC Nederland, High Tech Campus 48, PO Box 8550, 5605 KN Eindhoven.

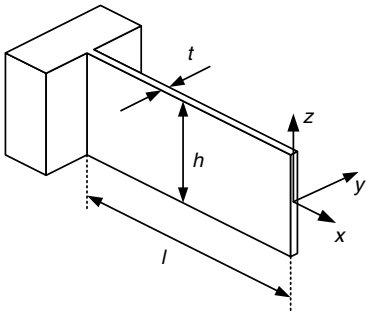

Figure 1. In-plane plate spring.

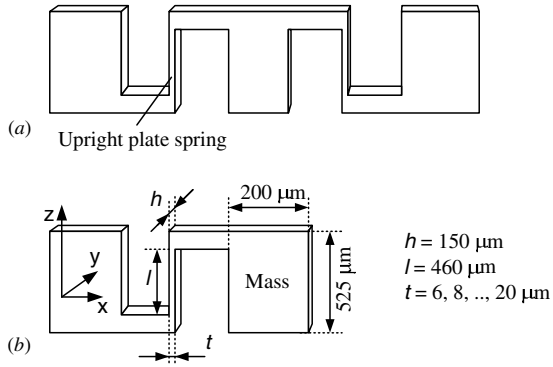

Figure 2. Schematic view of (*a*) an application example of upright plate springs, a parallel guiding with two such springs and (*b*) the device fabricated in this work to characterize upright plate springs.

A plate spring is generally thin, long and $h < l$. Modeling the plate spring (figure 1) as a slender beam, the stiffness in the x-, y-, and z-directions can be approximated by [7]

$$k_x = \frac{Eht}{l}, \tag{1}$$

$$k_y = \frac{Eht^3}{4l^3}, \tag{2}$$

$$k_z = \frac{Eth^3}{4l^3}. \tag{3}$$

Here E, h, t, and l are Young's modulus, the spring height, the spring thickness and the spring length, respectively. When we compare the ratios k_x/k_y and k_z/k_y (compliance versus support stiffness), we see that $k_x/k_y = 4l^2/t^2$ and $k_z/k_y = h^2/t^2$. By increasing h the ratio k_z/k_y can be increased, but at the price of reducing the compliance. On the other hand, by increasing l both the ratio k_x/k_y and the compliance can be increased. In theory k_x, k_y and k_z can be fixed independently, but when k_z has to be higher than k_x the resulting spring would have no practical use. Thus we conclude that the stiffness in the x-direction (k_x) is inherently higher than that in the z-direction (k_z). Therefore, in cases were the most stringent requirements are placed on the z-stiffness, a plate spring in the upright position (i.e., rotated 90° around the y-axis) should be used. The above-mentioned micro systems could profit from such an upright plate spring and an example of a parallel guiding system with upright plate springs is shown in figure 2(*a*). In this work, we will focus on the fabrication and characterization of a plate spring orientated upright in a silicon wafer. Using dual-side bulk micromachining, mass–spring systems like that shown in figure 2(*b*) are fabricated. The mass–spring resonance frequencies are used to characterize the performance of the plate springs. The characterization of a multi-parameter deep reactive ion etching (DRIE) process is well documented, for instance, by [8]. The same applies on the influence of the non-uniformity and etch profile shape on mechanical performance of bulk micromachined devices [9, 10]. Therefore, we only focus on the issues specific to the dual-sided fabrication process described in this paper. As will be explained in section 4, the sets of reference and mirrored single plate spring–mass systems allow us to discriminate dual-side etch errors from dual-side lithographic alignment errors. In fact, the sets of reference and mirrored devices can be used, not only as a basic element but also as a process control module in the study of basic construction elements. Our aim is to research such basic elements and form a generic component library for silicon-based flexible guiding mechanisms. This library should increase the design freedom and it will greatly simplify the future development of a large variety of micro systems.

2. Mechanical characterization

Resonance frequency measurements are used to determine the stiffness of the plate springs, which is an important device parameter. From the stiffness the corresponding spring thickness can be calculated. The relation between the resonance frequency (ω) and stiffness (k) is given by

$$\omega^2 = \frac{k}{m}, \tag{4}$$

where m is the mass attached to the spring. To measure the resonance frequencies of the devices, the dies are mounted on a shaker. The mechanical response of our plate spring system to the shaker excitation is measured with a laser vibrometer. By determining the smallest frequency step which still resulted in a noticeable difference in amplitude, it was found that the frequency can be measured with an accuracy better than 10 ppm. This measurement accuracy is higher than required, since model simplifications, temperature-dependent material properties and fabrication tolerances will result in a larger mismatch between resonance frequencies predicted by the model and the measured values.

We only consider the resonance mode where the mass is moving more or less linear along the x-axis, because this mode shape is similar to that of a plate spring in a parallel guiding. With the beam equations from [7], we can derive the equations describing the motion of the system, and analytically calculate the resonance frequency. We find that in this particular resonance mode the rotation of the mass is neglectable, and thus the same applies to its influence on the resonance frequency. After rewriting the appropriate stiffness is approximated by

$$k = \frac{Eht^3}{l^3}. \tag{5}$$

The resonance frequency is a function of m, h, l and t. However, in our test device, the mass and the stiffness both linearly depend on h, and thus cancel out each other. The values for h and those that determine m are determined by mask

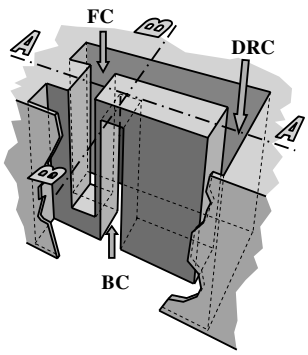

Figure 3. Schematic 3D view of the mass–spring system with upright springs.

layout, wafer thickness and DRIE under-etching. The value for l is determined by the DRIE etch rate. DRIE processes may vary over the wafer but in a close range, in the order of mm, these variations are negligible. Therefore it is assumed that the values for m, h and l are similar for a set of closely spaced devices. Furthermore, the dimensions of the mask layout and l are relatively large (>150 μm) compared to t (6–20 μm) and consequently t is the most sensitive parameter for process variations. This means that the resonance frequency of a set of closely spaced devices depends on a constant factor and the actual thickness. Rewriting the resonance equation,

$$\omega^2 = \frac{k}{m} = \frac{Eht^3}{ml^3} = \frac{Eh}{ml^3}t^3 \quad \Rightarrow \quad \omega^2 = B^3t^3 \tag{6}$$

with

$$B = \left(\frac{Eh}{ml^3}\right)^{1/3}. \tag{7}$$

In this paper, the mass–spring systems are characterized in groups. Within one group, the closely spaced devices have similar dimensions, such as spring height, spring length and mass and only the spring thickness is varied. Resonance frequency measurements of devices in one group are measured and equation (6) used is to calculate the corresponding thickness. However, in the case of non-uniform plate springs, this calculated thickness must be considered as an effective thickness, rather than a physical thickness.

3. Process description

The fabrication of an upright plate mass–spring system as given in figure 2(*b*) requires two technologies: ASML[4] 3D-align™ and deep reactive ion etching. 3D-align™ is an extension of the sub-micron alignment capabilities of an ASML wafer stepper that allows front-to-backside wafer alignment (FTBA). DRIE is used to etch deep cavities, aligned and etched on both sides of the wafer to form the upright plate spring as schematically depicted in figure 3.

Three lithographic masking layers are required to fabricate the upright plate spring–mass system: one layer to define the front-side cavity (FC), and the second layer to define the backside cavity (BC). The third layer, the device release

[4] ASML is a manufacturer of lithographic equipment for integrated circuit manufacturing (www.asml.com).

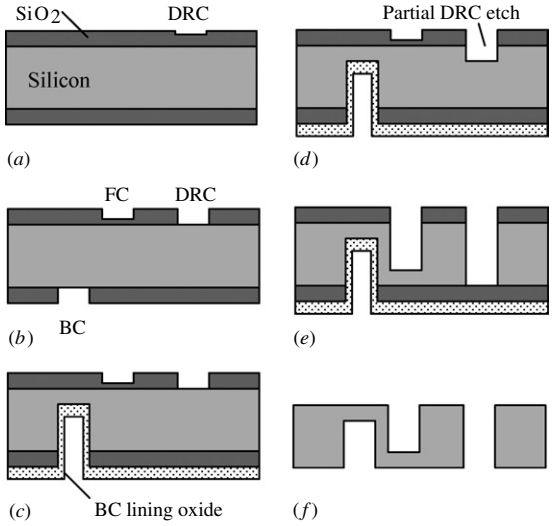

Figure 4. Device fabrication process flow; expose and etch the DRC 1.5 μm into the PECVD oxide hard mask (*a*). Expose the FC and BC masks. Next etch the oxide until it is completely removed at the BC and DRC, but 1 μm is left at the FC (*b*). DRIE of the silicon to give the BC and deposit 6 μm lining oxide on the backside of the wafer (*c*). The DRC is etched 100 μm into the silicon (*d*). Remove the remaining FC oxide and DRIE of silicon to create the FC and to continue the etching of the DRC areas (*e*). Remove the remaining lining and masking oxide to release the device (*f*).

cavity (DRC), is used to etch through the wafer in order to release the device from its surrounding silicon.

An overview of the process flow is given in figure 4 where the cross section A–A (see figure 3) is shown in different stages in the process. The fabrication starts with the deposition of 6 μm plasma enhanced chemical vapor deposition (PECVD) silicon oxide on both sides of a 525 μm thick, 100 mm diameter, double-sided polished silicon wafer (see figure 4(*a*)). This oxide serves as a hard mask for the DRIE process. First only the DRC mask is exposed and 1.5 μm of oxide is etched (figure 4(*a*)). After exposing the BC and FC masks, the BC layer is etched through the oxide. The remaining oxide is removed at the DRC with a shorter oxide etch (5 μm), which leaves 1 μm of oxide at the FC layer (figure 4(*b*)). All the required masking layers are etched in the masking oxide before any DRIE cavity is processed. This allows all the lithography steps to be completed using conventional wafer handling.

As mentioned before, DRIE is used to etch cavities deep into the silicon or even through the whole wafer. A high silicon etch rate requires high plasma power level in the DRIE etcher. Consequently, the thermal load on the wafer is high and enhanced wafer cooling is a prerequisite. Backwafer He gas cooling is commonly used to remove the heat from the wafer (see figure 5(*a*)). In fact, the wafer seals off the He cooling channels in the wafer chuck. Loss of He pressure will result in loss of temperature control and a reduced DRIE process performance. Therefore, a gastight wafer without open through wafer holes is mandatory throughout the whole process flow. Particularly the DRC etch needs attention on this point. To prevent He leakage a DRC etch-stop oxide and a BC lining oxide are needed in this process step. In figure 5(*b*) these oxide layers are drawn in the cross section B–B (see figure 3).

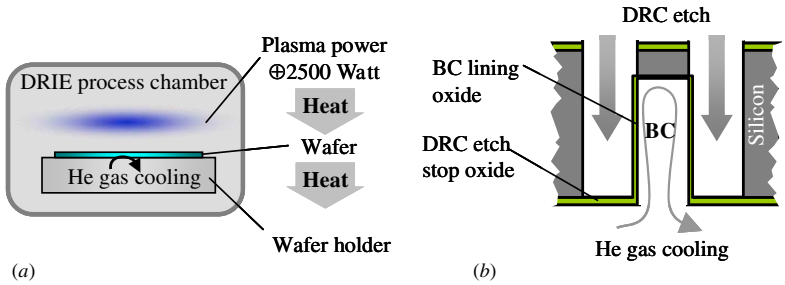

Figure 5. The principle of He backside cooling in a high power DRIE tool (*a*) and the use of BC lining oxide and DRC etch-stop oxide to prevent He leakage (*b*).

(This figure is in colour only in the electronic version)

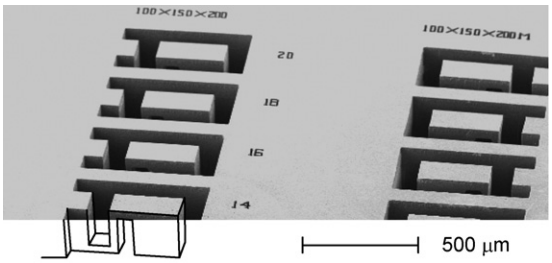

Figure 6. A SEM picture of a set of springs showing both the reference (left) and mirrored (right) devices. The drawing is added to the SEM picture to clarify the position of the spring.

Table 1. Process parameters used for the fabrication of upright plate springs.

Process	Parameters
PECVD hard mask	TEOS, 1.8 sccm, 2.9 mBar, 350 °C, RF power 500 W, LF power 500 W at 280 kHz
Hard mask oxide etch	C_2F_6 36 sccm, CHF_3 144 sccm, 16 mBar, RF power 300 W
DRIE (Bosch process)	SF6 700 sccm 7 s, C4F8 250 sccm 2 s, ICP power 2000 W

The BC areas are etched 480 μm deep into the backside of the wafer followed by a BC lining oxide deposition using PECVD (see figures 4(*c*) and 5(*b*)). Next the DRC is etched 100 μm into the silicon; the remaining FC oxide blocks the silicon etch in the FC areas (figure 4(*d*)). After the DRC silicon etch, the remaining FC oxide is removed using a maskless oxide RIE. In the next step, both the FC and DRC areas are further etched. This etch is continued until all the DRC silicon is removed (figure 4(*e*)). The BC masking oxide at the backside of the wafer serves as a etch-stop layer for the DRC etch. After the DRC etch, about 30 μm silicon is left in the FC areas to connect mass to the upright plate spring. Finally, the remaining oxide is removed using wet chemical etching to release the devices (figure 4(*f*)). Details on the etch recipes used are given in table 1. A set of fabricated springs are shown in figure 6.

4. Fabrication technology

FTBA accuracy plays a crucial role in the process described in the previous section. The designed thickness of the spring (t_0, see figure 7(*a*)) is directly affected by the front-to-backside alignment error (t_1, see figure 7(*b*)). The FTBA accuracy has been investigated in the previous work [11] and is verified using FTBA calibration procedures [12]. The current FTBA accuracy on the ASML PAS5000/50 wafer stepper, used in this work, is better than 500 nm.

The effect of the DRIE process on the spring thickness is more complicated. In the first place the spring thickness is affected by the shape of the DRIE profile. For example, a positive side-wall slope results in an increased thickness (see figure 8(*a*)); nevertheless, the thickness is constant over the entire length of the spring. Second, a non-perpendicular direction of the DRIE profiles can affect the spring thickness in a non-uniform way (see figure 8(*b*)).

Although DRIE offers high anisotropy for very deep structures, the profile direction might deviate from the ideal perpendicular direction. In our case, the etch depth is 480 μm. Consequently, a deviation of the ideal perpendicular direction of only $\pm 0.1^\circ$ will result in a displacement of ± 0.8 μm at this depth.

The direction of the DRIE process can be investigated using electrical overlay measurements [13]. With this method, the front-to-backside overlay in a through wafer DRIE etch process is measured in the x-direction (see figure 9). Compared to the target spring thickness (10–20 μm), the measured overlay error is significant. Consequently the direction of the DRIE profile will have a significant influence on the thickness and shape of the plate spring.

The effect of FTBA errors, DRIE profile inclination and DRIE profile shape on the resonance frequency is simulated using ANSYS®; the overall dimensions of the mass–spring system are given in figure 2(*b*). For FTBA errors, the results are summarized in figure 10.

As expected, the variations in spring thickness correspond with the change in the resonance frequency; for example, a 10 μm nominal width spring with an alignment error of 2 μm yields the same frequency as a 12 μm spring with 0 μm alignment error.

The effect of DRIE profile shape and inclination is summarized in figure 11. Four different DRIE profiles are considered (see figure 11(*a*)); positive taper (device 1), negative taper (device 2) and inclined profiles (device 3 and 4). The corresponding resonance frequencies are given in figure 11(*b*).

Tapered DRIE profiles (devices 1 and 2) will either increase or decrease the spring thickness but will result in

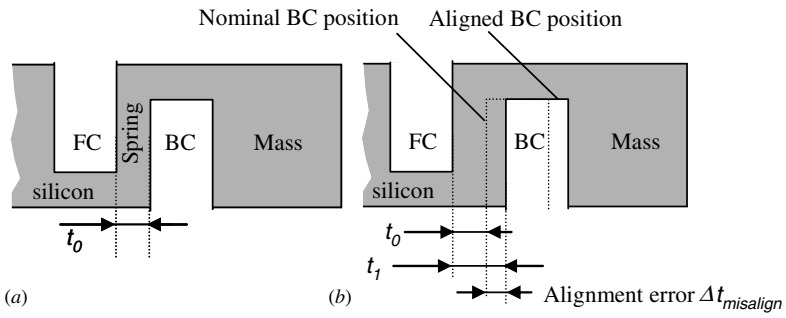

Figure 7. The effect of an FTBA alignment error on the spring thickness.

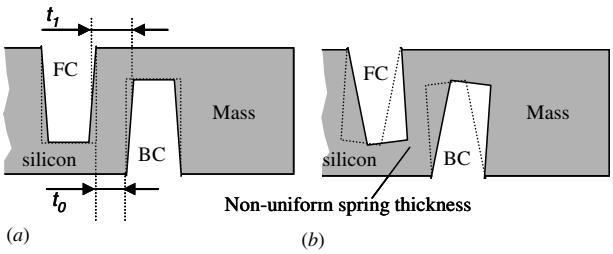

Figure 8. The effect of taper and non-perpendicular etch profiles on the spring thickness.

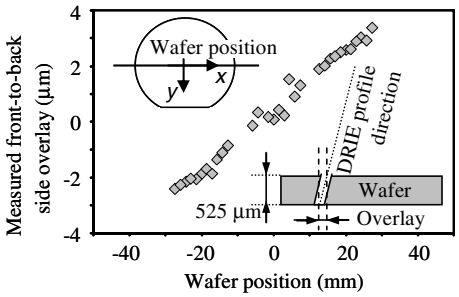

Figure 9. Front-to-backside overlay error after through-wafer DRIE, measured across the wafer center.

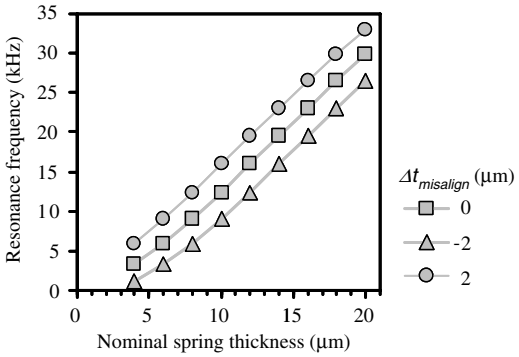

Figure 10. Calculated resonance frequencies for devices with different nominal spring thicknesses and FTBA alignment errors.

a uniform spring thickness, while inclined DRIE profiles will result in a non-uniform spring thickness either with the smallest part at the bottom or at the top. This does not lead to a large difference in device performance; the resonance frequencies of devices 3 and 4 do not differ that much. For example, the resonance frequency for devices with 10 μm nominal thickness is 12 629 Hz and 12 369 Hz for devices 3 and 4, respectively. Furthermore, the resonance frequency for a device with 10 μm uniform spring thickness is 12 407 Hz, close to the values of devices 3 and 4. Apparently non-uniform plate springs such as devices 3 and 4 behave as a uniform device with the corresponding average spring thickness.

To discriminate the effect of FTBA and DRIE on the final spring thickness, the mass–spring devices are fabricated in closely spaced sets of mirrored and non-mirrored (reference) devices. The devices are mirrored in the x-direction (see figure 12). Within one set, the distance between the two devices is less than 1 mm. Therefore we may assume that for both devices, the BC and FC DRIE profiles are similar. Hence, for both devices, the influence of the DRIE process on the spring thickness is the same.

However, within one set, a shift in the alignment error will introduce an asymmetrical change in the spring thickness (see figure 10). Thus the spring thickness of a set of mirrored and reference devices can be described by two equations with two variables:

$$\text{Reference:} \quad t_1 = t_0 + \Delta t_{\text{etch}} + \Delta t_{\text{misalign}} \tag{8}$$

$$\text{Mirrored:} \quad t_1 = t_0 + \Delta t_{\text{etch}} - \Delta t_{\text{misalign}}. \tag{9}$$

Here t_0, Δt_{etch} and $\Delta t_{\text{misalign}}$ are the nominal spring thickness, the error caused by DRIE and the error caused by FTBA misalignment, respectively.

Considering equations (6), (8) and (9), the resonance frequencies for the reference and mirrored devices can be expressed as follows:

$$\text{reference:} \quad \omega^{2/3} = B(t_0 + \Delta t_{\text{etch}} - \Delta t_{\text{misalign}}) \tag{10}$$

$$\text{mirrored:} \quad \omega^{2/3} = B(t_0 + \Delta t_{\text{etch}} + \Delta t_{\text{misalign}}). \tag{11}$$

The factor B is inverse proportional to the spring length (see equation (7)) and the actual value of l depends on the DRIE etch rate. Consequently B might vary from its theoretical value, due to etch rate non-uniformity, so it is best calculated from the measurement results. However, the three unknowns, B, Δt_{etch} and $\Delta t_{\text{misalign}}$, cannot be solved with only two equations. Therefore, a number of identical mass–spring systems with different t_0 are grouped together with the corresponding mirrored devices. The devices in a group are closely spaced; hence the process variations are very small within one group and a least-squares fit can be used to extract the average values of B, Δt_{etch} and $\Delta t_{\text{misalign}}$. The results are discussed in section 5.

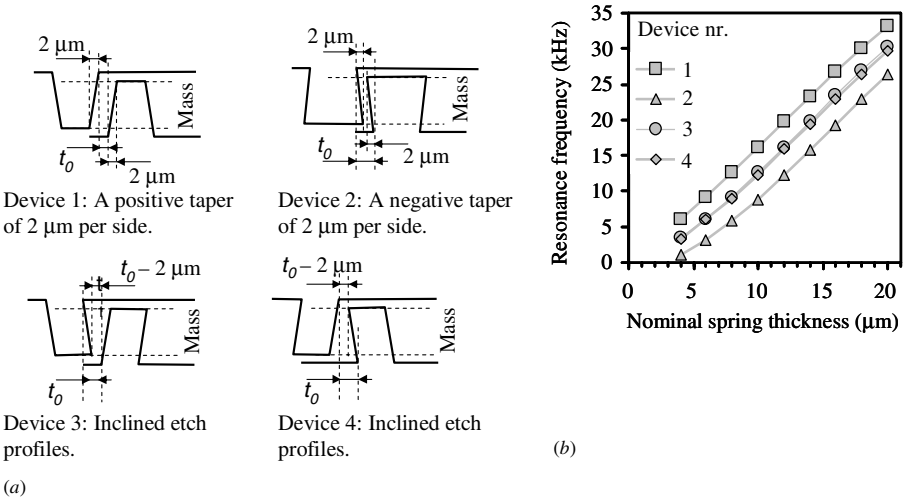

Figure 11. Calculated resonance frequencies for devices with different DRIE profiles.

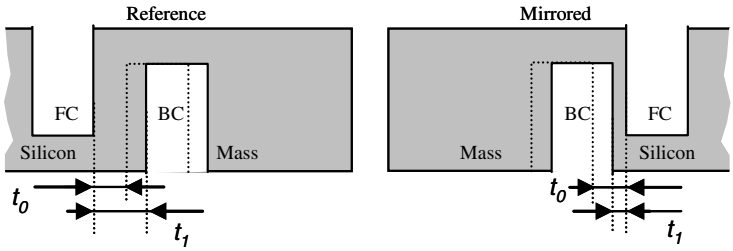

Figure 12. The asymmetrical effect of FC to BC alignment errors on the spring thickness.

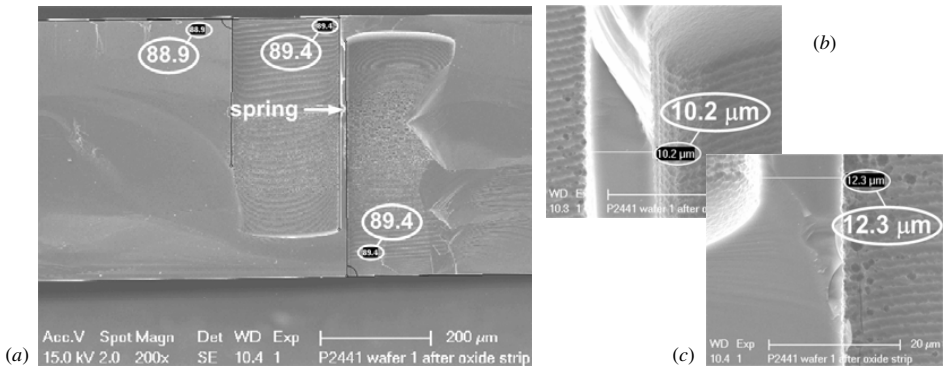

Figure 13. SEM cross section of a device without release cavity (*a*). The angles show the taper and the inclination of the etch profile. The close-ups ((*b*) and (*c*)) show the difference in the spring width at the top and the bottom due to the inclined etch profile.

5. Result and discussion

Three groups with sets of mirrored and reference devices are measured on three different locations across the wafer center (see figure 9). The dimensions of the spring within one group are $l = 460\ \mu$m, $h = 150\ \mu$m and $t_0 = 10$–$20\ \mu$m in steps of $2\ \mu$m. The results are summarized in table 2.

The variations in B are caused by the DRIE etch rate non-uniformity. The silicon etch rate of groups I and III are 0.6% higher compared with group II, which corresponds with the higher value for B for group II. The fitted $\Delta t_{\text{misalign}} < 0.4\ \mu$m which is within the specifications of the wafer stepper; however Δt_{etch} varies considerably.

Most likely, DRIE under-etching and/or tapered DRIE profiles, as shown in figure 11(*a*) (device 1), are responsible for the relative large value of Δt_{etch}. Figure 13(*a*) shows a cross section of a device fabricated without release cavity (otherwise the spring would not survive). The measured angles show that the etch profile is tapered and slightly inclined. Figures 13(*b*) and (*c*) are close-ups of the top and bottom of the spring. The

Table 2. Fitted model parameters of three identical groups at different positions across the wafer center.

Group number	Wafer position (mm)	B ($\text{m}^{-1}\ \text{s}^{-2/3}$)	$\Delta t_{\text{misalign}}$ (μm)	Δt_{etch} (μm)
I	−12	1.79×10^8	0.15	−1.91
II	3	1.87×10^8	0.38	−0.30
III	18	1.80×10^8	0.08	−2.94

Table 3. Measured resonance frequencies, calculated stiffness and effective thickness for resonance in the x-direction of the devices from group II.

Nominal thickness (μm)	Resonance frequency (Hz)	Calculated stiffness (N m^{-1})	Calculated thickness (μm)	Thickness error (%)
20	36 414	1921	19.98	−0.10
18	30 952	1388	17.93	−0.39
16	26 703	1033	16.25	1.56
14	22 501	733	14.49	3.50
12	17 170	427	12.10	0.83
10	12 873	240	9.99	0.10
8	9 186	122	7.98	−0.25
6	5 610	46	5.74	4.33

spring is wider at the bottom than at the top, which is caused by the inclined etch profile.

For the second group the calculated spring stiffness and effective thickness are shown in table 3. In the case where $\Delta t_{\text{misalign}}$ compensates Δt_{etch}, the calculated effective thicknesses are very close to the nominal thickness. This is demonstrated by the mirrored devices of group II (see table 3). The largest found error is only about 4%. This demonstrates that at least the devices close to the center of the wafer are fabricated with low tolerances, and their stiffness is close to the designed value.

6. Conclusions

High aspect ratio dual-side processed upright plate springs are successfully fabricated using a combination of two technologies: FTBA and DRIE. The plate springs are characterized by the resonance frequency measurement of the mass–spring system as shown in figure 2(*b*). Furthermore, a novel method that employs the asymmetry of reference and mirrored mass–spring systems is presented to discriminate align and etch errors; as such this method can be used as a process control module in the fabrication of more complex devices.

Using this method, we found that FTBA accuracy is not the limiting factor. Most likely, under-etching and the shape of the DRIE profile are mainly responsible for deviations of the spring thickness across the wafer. The inclination of the DRIE profile will result in a non-uniform spring thickness, but ANSYS® simulations showed that the effective spring thickness is close to the nominal value. However, the reduced thickness at one side of the spring might affect the device reliability due to, for example, stress concentrations. This was not yet investigated, but will be considered in future work.

Devices with close to nominal dimensions are fabricated near the wafer center, particularly for the case where the $\Delta t_{\text{misalign}}$ compensates Δt_{etch}. This demonstrates the ability of this technology to fabricate a parallel guiding system with upright plate springs (for an example, see figure 1) with low tolerances. This is a necessity for the successful development and application of such guiding mechanism in high precision positioning systems. Particularly this class of positioning systems can benefit strongly from the high stiffness of the upright plate spring. However, future improvement of the DRIE process is required to fabricate good devices across the whole wafer.

Aknowledgments

The authors would like to thank Dr H Krikhaar and W de Laat from ASML for their support.

References

[1] Xie H and Fedder G K 2003 Fabrication, characterization, and analysis of a DRIE CMOS-MEMS gyroscope *IEEE Sensors J.* **3** 622–31

[2] Marxer C, Tio C, Grétillat M-A, de Rooij N F, Bättig R, Anthamatten O, Valk B and Vogel P 1997 Vertical mirrors fabricated by deep reactive ion etching for fiber-optic switching applications *J. Microelectromech. Syst.* **6** 277–85

[3] Syms R R A, Lohmann A and Huang W 2006 Extended range tuning elements for a microelectromechanical systems external cavity laser *J. Opt. A: Pure Appl. Opt.* **8** 299–304

[4] Maloney J M, Schreiber D S and DeVoe D L 2004 Large-force electrothermal linear micromotors *J. Micromech. Microeng.* **14** 226–34

[5] Hirano T *et al* 1998 High-bandwidth high accuracy rotary microactuators for magnetic hard disk drive tracking servos *IEEE/ASME Trans. Mechatron.* **3** 156–65

[6] Brouwer D M, de Jong B R, Soemers H M J R and Van Dijk J 2006 Sub-nanometer stable precision MEMS clamping mechanism maintaining clamp force unpowered for TEM application *J. Micromech. Microeng.* **16** S7–12

[7] Gere J M and Timoshenko S P 1993 *Mechanics of Materials* 3rd SI edition (London: Chapman and Hall) pp 771–3

[8] Ayón A A, Braff R, Lin C C, Sawin H H and Schmidt M A 1999 Spatial variation of the etch rate for deep etching of silicon by reactive ion etching *J. Electrochem. Soc.* **146** 339–49

[9] Chen K S, Ayón A A, Zhang X and Spearing S M 2002 Effect of process parameters on the surface morphology and mechanical performance of silicon structures after deep reactive ion etching (DRIE) *J. Microelectromech. Syst.* **11** 264–75

[10] Pike W T and Kumar S 2005 Effect of profile shape on mechanical performance of silicon lateral suspension *Proc. 16th MicroMechanics Europe Workshop (Göteborg, Sweden)* pp 34–7

[11] Van Zeijl H W, Bijnen F G and Slabbekoorn J 2004 Characterization of waferstepper and process-related front- to backwafer overlay errors in bulk micromachining using electrical overlay test structures *Proc. SPIE* **5455** 398–406

[12] Smeets E M, Bijnen F G, Slabbekoorn J and Van Zeijl H W 2004 3D align overlay verification using glass wafers *Proc. SPIE* **5641** 152–62

[13] Van Zeijl H W and Slabbekoorn J 2003 Characterization of front- to backwafer alignment and bulk micromachining using electrical overlay test structures *Proc. SPIE* **5116** 617–26